TUDelft

Delft University of Technology

Design of a concept wedge-shaped self-levelling railway sleeper

Jia, Wenli; Markine, Valeri; Carvalho, Mario; Connolly, David P.; Guo, Yunlong

Citation (APA)
Jia, W., Markine, V., Carvalho, M., Connolly, D. P., & Guo, Y. (2023). Design of a concept wedge-shaped self-levelling railway sleeper. *Construction and Building Materials*, *386*, Article 131524. https://doi.org/10.1016/j.conbuildmat.2023.131524

Important note
To cite this publication, please use the final published version (if applicable).
Please check the document version above.

Design of a concept wedge-shaped self-levelling railway sleeper

Wenli Jia [a], Valeri Markine [a], Mario Carvalho [a,b], David P. Connolly [c], Yunlong Guo [a,*]

[a] Faculty of Civil Engineering and Geosciences, Delft University of Technology, Delft 2628CN, the Netherlands
[b] ProRail, Utrecht 3511EP, the Netherlands
[c] School of Civil Engineering, University of Leeds, UK

ABSTRACT

Differential railway track settlement can result in ballast voids, leading to sleepers that hang from the rail and are no longer supported by the ballast. These hanging sleepers are damage for track component. As a solution, this paper proposes and investigates a new concept sleeper with a wedge-shaped geometry, intended to stimulate the migration of ballast into any voids, thus reducing the occurrence of hanging sleepers. A series of scaled laboratory tests and 2D and 3D discrete element simulations are used to investigate different wedge-shaped geometries. The investigations include the wedge type (single long wedge versus multiple mini-wedges) and the wedge angle (30, 45, 60 degrees). First, the scaled laboratory tests are used to study the performance of different wedge geometries. Next, 3D DEM simulations are performed to analyse the contact forces in the ballast due to different wedge designs. Finally, 2D DEM simulations are performed to study the settlement behaviour. The main conclusions are that a single long wedge is preferable compared to multiple smaller wedges. when the wedge sleeper angle is larger than the ballast's angle of repose, particles have the freedom to migrate into the settlement induced voids. Also, an increased wedge sleeper angle stimulates greater particle migration and thus improves the support correction. However the longer wedge also leads to a decrease in effective ballast height under sleeper which may make retrofitting on existing lines challenging.

1. Introduction

Railway tracks are supported by a variety of types of sub-structures, including subgrade, bridges, and tunnels. The connecting area between support structures with different stiffness's is named a transition zone [1,2]. As an example, when trains travel over a transition zone from an embankment to a concrete abutment, the change in stiffness leads to differential settlement. This can result in hanging sleepers that are unsupported by the ballast layer [3]. Both differential settlement and hanging sleepers constitute geometry irregularities. An overview of those problems is shown in Fig. 1.

When a train passes unsupported sleepers, their impact on the ballast surface when excited generates a dynamic force, thus further enlarging the differential settlement and voids [3–5]. This results in a progressive degradation loop. Track irregularities are an important contributor to the increase in dynamic loads [6–8], and compared with plain line, the degradation of ballast and other track components at transition zones is much faster. Thus higher maintenance costs are needed to ensure the safety and stability of the railway [9].

A variety of studies have proposed preventive solutions to decrease the differential settlement by lowering the dynamic force and the plastic deformation within the ballast layer on the embankment side. These solutions focus on smoothing the stiffness change in transition zones [10–14] because sudden stiffness changes result in high dynamic forces [15–18]. In addition, reinforcement on the ballast layer increases it's strength [19–22], thus increasing it's resistance to deformation.

However, the above preventive solutions still have some challenges [23,24]. Also, after implementing these solutions, hanging sleepers can still develop and produce high dynamic forces. To eliminate these, maintenance actions are performed, such as tamping/stone blowing [25] and using adjustable fasteners [26]. However, these manual actions can be costly, short-lived and also some maintenance activities (e.g. tamping) can be challenging to perform at certain transition zone configurations.

In an attempt to prevent the development of hanging sleepers the Automatic Irregularity-Correcting Sleeper (AICS) was developed [27], capable of expanding in the vertical direction to fill the void and thus ensure contact between ballast and sleeper. The AICS consists of two automatic subsidence compensating (ASC) mechanisms. The ASC device consists of two nested boxes. When there is differential settlement in the
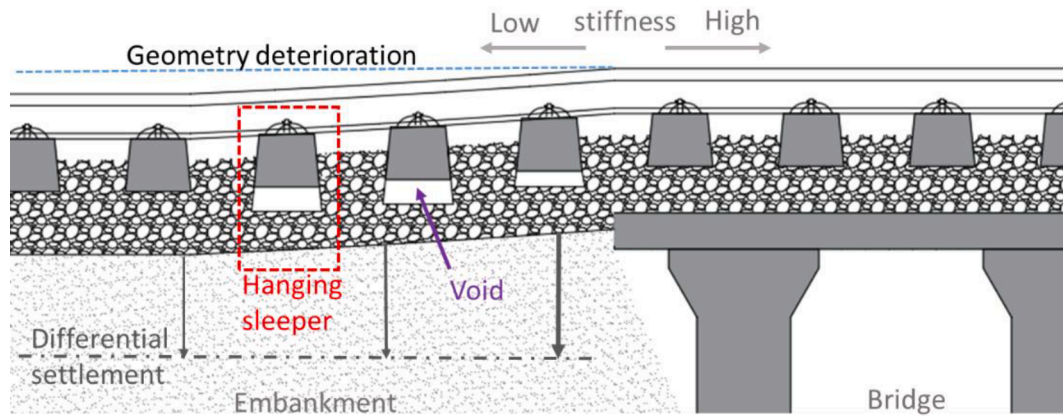

Fig. 1. Differential settlement and hanging sleepers at a transition zone. Modified from Paixão et al. [3].

track, the outer box sinks together with the ballast, with a granular material (e.g. stainless steel ball bearings) filling the gap between the inner and outer boxes. As a result, the granular material compensates for the unequal settlement. To minimise installation time, and negate the need to remove the existing sleepers, an alternative short-sleeper version (AICS-SS) was developed [28]. It could be more easily installed and could be placed between existing sleepers.

Another Self-Compensating Sleeper (SCS) concept using granular material is presented in Insley and Sharpe [29]. The SCS has conical shaped cavities from the top surface to the bottom that house granular material with smaller particle size distribution compared to ballast. When the track is lifted, the granular material in the sleeper cavities falls into the cavities under the sleeper, thus helping to fill the voids and maintain sleeper-ballast contact.

In contrast to using granular compensation mechanisms, an alternative was proposed using automated air-bag technology [30]. When the ballast settles, the air bag restricts movement in the opposite direction by air injection. This helps to minimise gaps between the sleeper and the ballast. Another alternative proposed using hydraulic oil under pressure to automatically compensating for the loss of sleeper-ballast contact during track differential settlement [31].

The above solutions are useful for preventing the growth of voids at transition zones, however are semi-active solutions and may have increased cost compared to a standard sleeper. Further, they may require resetting after they have met their vertical expansion limit. Passive solutions may help overcome these issues, for example by using a dual ballast gradation approach [32–35]. This involves first installing ballast with standard PSD up to the sleeper bottom level. This will ideally be well-compacted to provide a solid foundation for the sleeper. Then, the crib/shoulder ballast above, which is more for confinement rather than vertical support, is installed, but with a smaller PSD. Then, if voiding starts to develop, the smaller upper crib/shoulder particles automatically migrate into the voids to minimise their growth.

A challenge with using a dual-gradation approach is that it can be challenging to ensure compatibility with railway standards. Therefore, as an alternative, this paper proposes the use of a wedge-shaped sleeper. The concept is that the wedge allows larger particles to flow between it and any voids that may develop. Therefore it increases the contact between sleeper and ballast. To design a wedge sleeper, first the concept is explained in detail, and the working principle and challenges in design are presented. Next the methodology is described, including the scaled laboratory tests, 3D and 2D DEM simulations. Then, the analysis of the results, including the influence of wedge type (single-wedge and multi-wedge) and the wedge angle (30, 45 and 60-degree) on the support correction effect are presented.
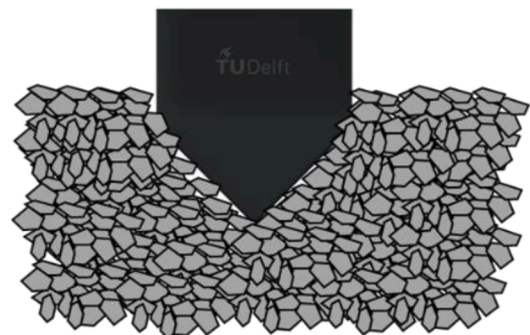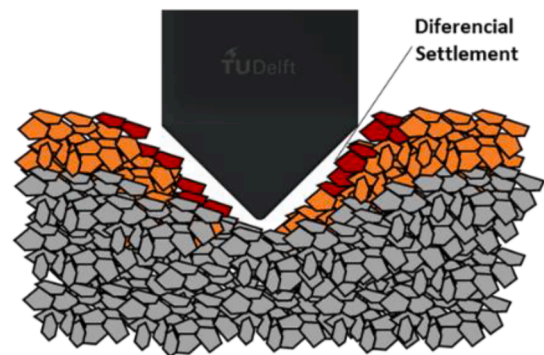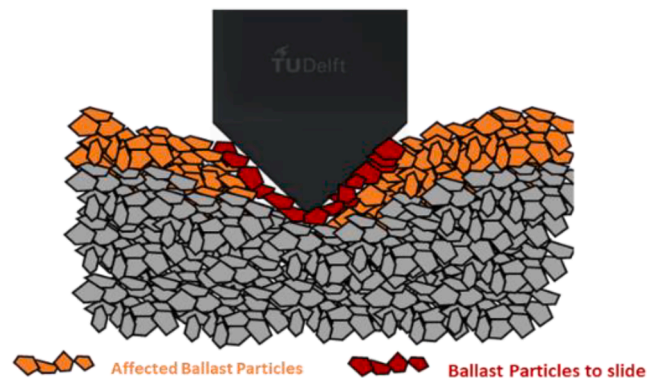

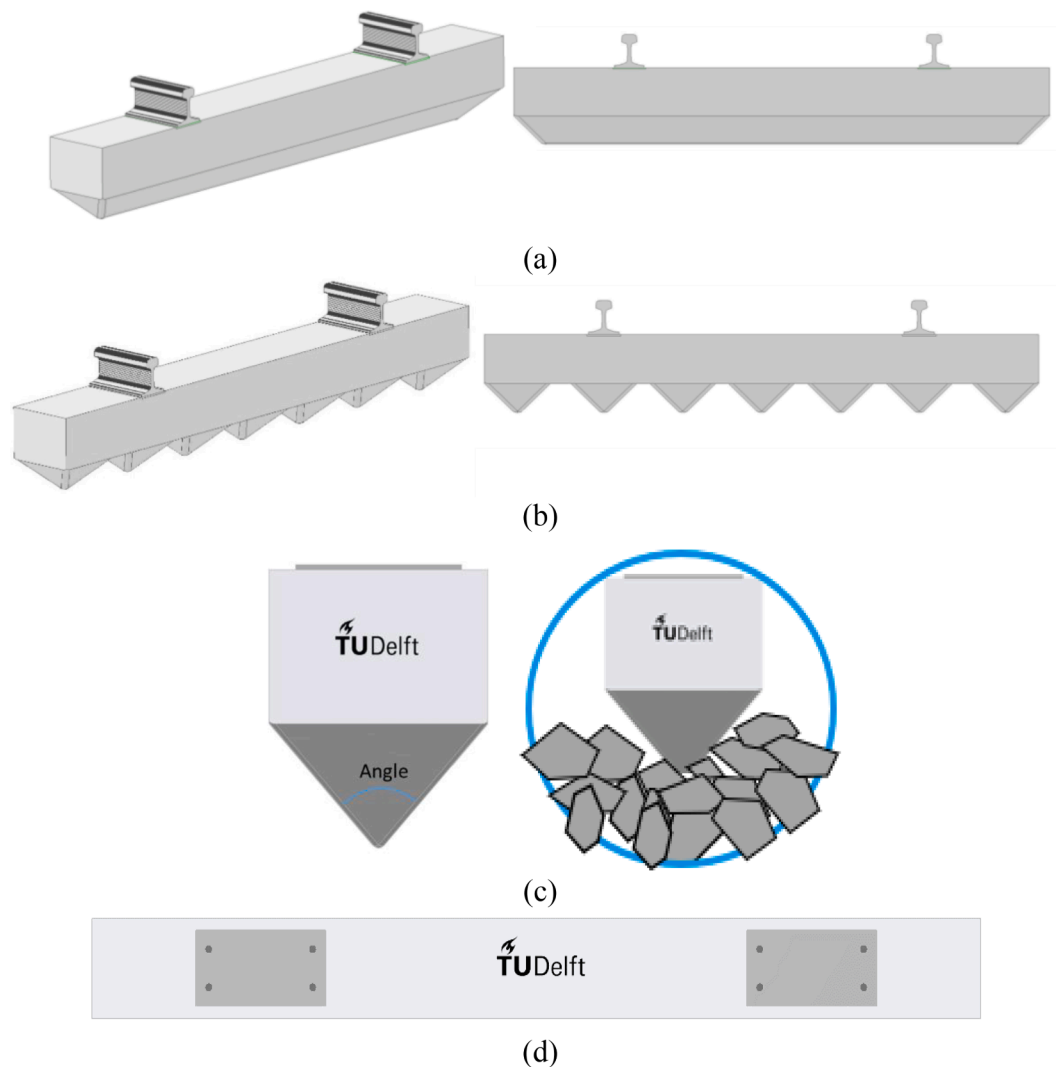**Fig. 2.** Void correction concept using wedge sleeper.

Fig. 3. Wedge-sleeper designs. (a) Single wedge design, (b) Multi-wedge design, (c) Side-view of both designs, (d) Top-view of both designs.

2. Wedge sleeper concept

The rail is fixed to the sleeper via a clip meaning in the presence of differential ballast settlement a gap can appear between the sleeper and ballast. The working principle of the wedge sleeper is that the crib and shoulder ballast can, via gravitational forces and dynamic vibration during train passage, migrate into the gap between sleeper and ballast. The wedge shape helps to promote the migration of ballast, which works autonomously and is related to the angle of repose of the ballast. The correction behaviour is illustrated in Fig. 2.

Two designs for the wedged sleeper were tested. First, the single wedge was tested, which is the simplest design to promote ballast migration underneath the sleeper. The multiple wedge solution follows the same principle while also aiming for material saving and allowing particle flow in two directions. Therefore potentially both lateral and longitudinal ballast migration can contribute to correction. The design of full-scale sleepers is shown in Fig. 3. The idea of improving sleeper performance by adding extra components has been used in several designs [36,37]. In this paper, the prototypes are based on the existing mono-block sleeper (Lankorst type 202), with a dimension of 2600 mm*250 mm*200 mm (L*W*H). It is High-Density Polyethylene Polymer (HDPE) with reinforcing bars. The material is flexible to modification to meet the requirements, such as weight, strength, and dimension of reinforcement.

Some key design parameters of the wedge(s) are the angle and

height. For example, when the angle is larger than the repose angle of the ballast, the displacement and rotation of the ballast can contribute to void correction. Thus, the wedge angle is crucial to the design. In general, a larger angle increases the possibility of ballast movement. However, this decreases the effective depth of ballast below the sleeper, thus weakening the function of the ballast, for example, lowering the elasticity and strength. In addition, the sharper the tip of the wedge, the higher the force concentration on both itself and the ballast. This can cause accelerated degradation/breakage of both the tip and ballast stones. Therefore these issues are investigated in this paper.

3. Methodology

3.1. Overview

This paper aims to use a combination of scaled laboratory testing and discrete element modelling (2D and 3D) to investigate:

1. Performance of different wedge types. Scaled laboratory tests are used to investigate both single and multi-wedge designs. The tests provide understanding of general wedged sleeper behaviour.

2. Performance of different wedge angles. 3D discrete element modelling is used, capable of simulating the contact between the sleeper and ballast. It is used to study the effect of wedge angle and the relationship between ballast migration and sleeper height.

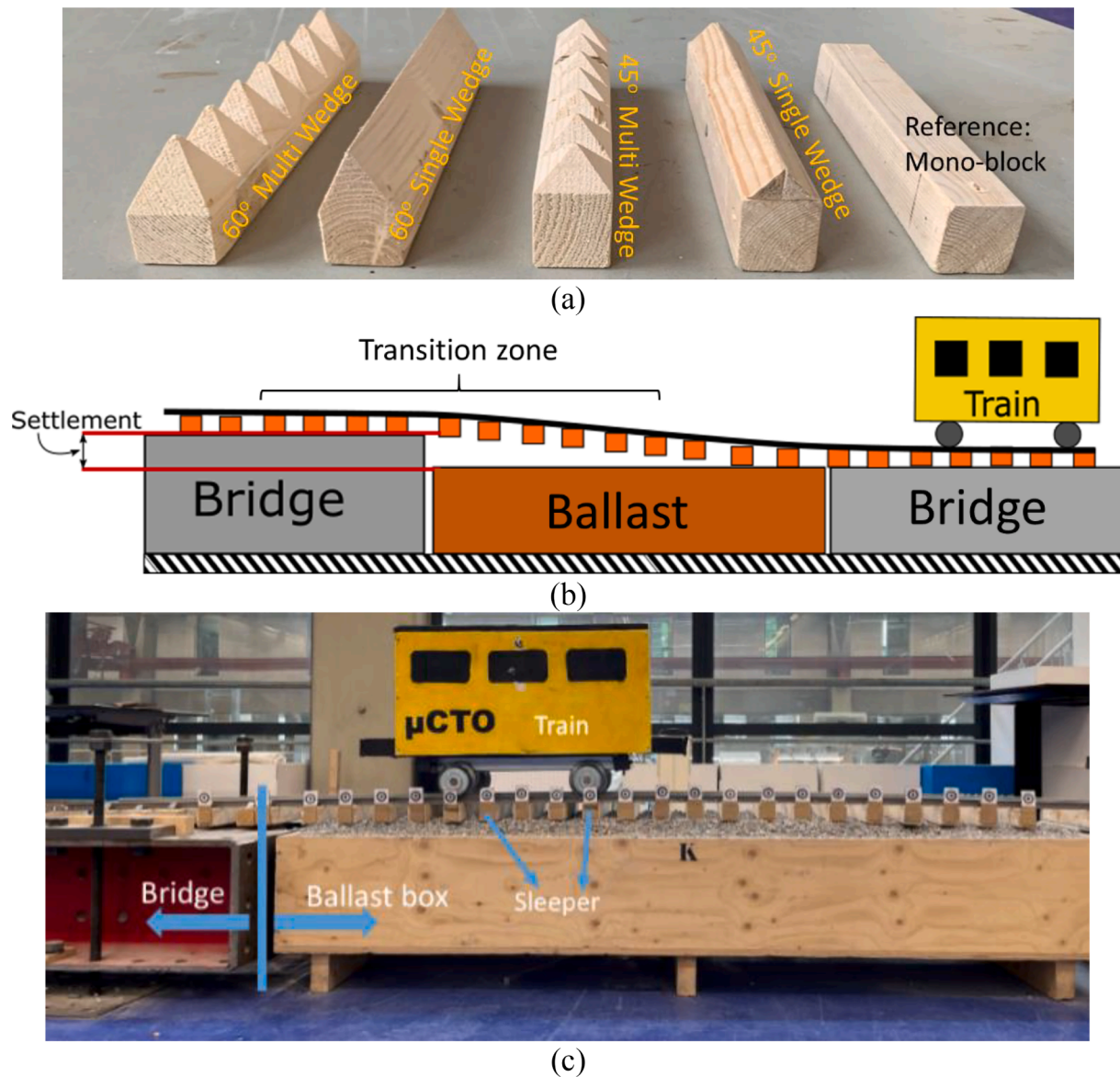3. The effect of support correction effects: validating the predicted

(a)

(b)

(c)

Fig. 4. Scaled testing. (a) 5 different types of sleepers under test, (b) Schematic of the scaled laboratory transition zone, (c) Final laboratory model.

correction under different settlement levels, and the influence of the correction behaviour on the force state of sleeper and ballast layer. To study the long-term behaviour under different settlement levels, 2D discrete element modelling is used.

The laboratory testing and numerical simulations are now described.

3.2. Laboratory testing

First, scaled laboratory testing was used to investigate wedge angles and types (single or multi-wedge), with a mono-block sleeper used as a reference. Wooden sleepers with the dimensions 300x45x45mm were used, comparable with the typical sleepers used in the Netherlands, with a scale factor of 1:7.5. The rails were U profiles (channel steel) of 10x20x10mm. Thus, to evaluate the settlement correction of the TU Delft Sleeper designs, their scale was set as approximately the same as one of the ballast particles. The relationship between the average ballast particle dimension (40 mm) and the gravel particle (6 mm) was 1:6.6.

A retaining box of 1900 × 700 × 250 mm was filled with gravel to act as ballast. A steel beam, of 300 mm of height, is used to replicate a bridge, thus creating a transition zone between the ballast and bridge. At the beginning of the tests, the steel beam is lifted 10 mm to introduce the

initial differential settlement. The sleepers under test are shown in Fig. 4a, and the scaled transition zone is shown in Fig. 4b and c. The scaled train vehicle passed over the transition zone 16 times for each designs, and the displacement of sleepers was recorded using a video gauge system with targets placed on each sleeper end. Comparing the particle size, sleeper size, and the introduced settlement, the scaled tests provide an easier condition to qualify the correction. Under this condition, if the sleeper cannot show a good performance, the sleeper is considered to be even worse in reality. Thus, the scaled tests were only used to primarily qualify the performance.

3.3. Discrete element modelling

Discrete Element numerical simulation (DEM) was used to develop a detailed understanding of the contact behaviour between the sleeper and the ballast particles [38–40]. The cooperation between the 2D and 3D methods (co-simulations) is employed in this research.

Because of the huge calculation efforts, the 3D model is impossible to simulate a long-term time period, but the results are more accurate [41]. In comparison, the 2D models are time-saving but less accurate due to one dimension loss. The co-simulations are developed, which use the 2D
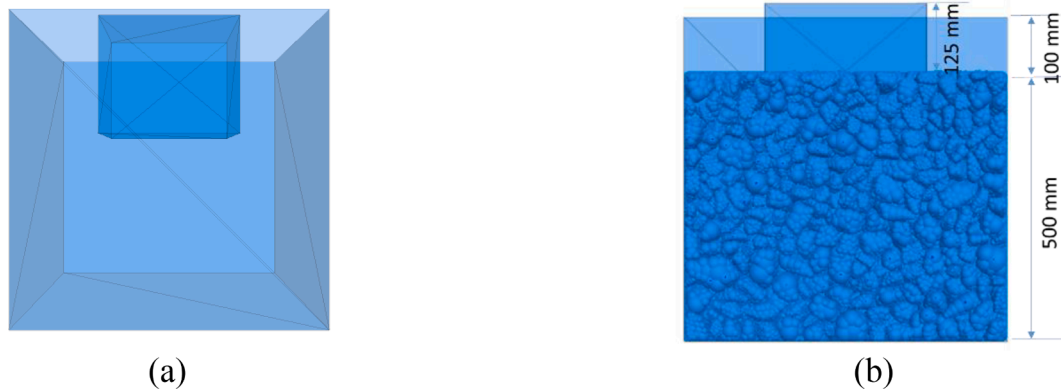
Fig. 5. Sleeper & Ballast box model. (a) Box and sleeper, (b) Box filled with ballast.

model as the supplement for the efficiency loss of the 3D model, and it uses the results of the 3D model as a resource of calibration to improve the reliability of the 2D model. This combination largely improves the feasibility of the DEM modelling method.

Also, due to the efficiency problems, different loading processes are applied. The 3D simulations used a 1-cycle loading, which is close to the quasi-statics process, mainly to obtain the contact behaviour between sleeper and ballast. Whereas the 2D models used cyclic loading, by which the repeated train loading and restriction from rail and fasteners are simulated, and the sleeper displacement is the main focus.

3.3.1. 3D model

The 3D model includes 3 parts: a box, ballast particles, and a sleeper, as shown in Fig. 5. The ballast particles are clumped elements, made by assembling several balls together to present one ballast particle. The ballast box and sleeper are wall elements, which are assemblies of triangle facets [42].

The 3D model is comprised of the following key parts:

1. The ballast box (formed from wall elements) is the container for the ballast particles, with dimensions: 600*600*600 mm. The box is filled with ballast clumps to 500 mm height. Wall elements. The walls contains the force condition, but cannot transmit forces to another side and move under unbalance forces. It is generated typically as the boundary.

2. Ballast particles (formed from 3D clump elements) are generated from 10 different templates, as shown in Fig. 6a. The templates were derived from real ballast particles using 3D scanning (Fig. 6b), which makes sure that the contact behaviour between ballast particles is reliable in geometry. The Particle Size Distribution (PSD) of the ballast particles in the ballast box is shown in Fig. 6c.

3. Sleepers (formed from wall elements) were simulated according to the different wedge geometries under test. The mono-block reference sleeper has dimensions 300*300*250 mm and also acted as the basis for the different wedge geometries (Fig. 7). Considering ballast's angle of repose ballast [40], the wedge angles were chosen as 30 degrees, 45 degrees, and 60 degrees. The height of the sleepers is a function of the wedge angle, and are: 87 mm, 150 mm, and 260 mm, respectively. Those sleepers are located at the same position by controlling the location of the sleeper top height, which is 125 mm higher than the ballast top surface, as shown in Fig. 5.

4. The contact model is used to define the force–displacement behaviour for ballast-ballast contact and ballast-wall contact. The linear contact model is used with the parameters listed in Table 1. All parameters were verified in earlier studies [43–46]. Additional details regarding the contact models and parameters can be found in [42].

The support correction effect was validated using a loading simulation with a pre-set settlement condition. Considering the computational cost of 3D DEM simulation, a 1 cycle loading process is used. It is

controlled by applying a positive or negative z-direction velocity (4 mm/ s) to the sleeper. The loading process was divided into 3 stages as shown in Fig. 8 (and Fig. 3):

Stage 1: Lift the sleeper 4 mm, for the purpose of introducing initial ballast settlement.

Stage 2: Stopping the sleeper movement at a fixed position, followed by time window to allow the ballast to move (under gravity) and fill the ballast-sleeper void. The time window was controlled with 50 k calculation cycles to ensure the ballast movement was sufficient. Note that the calculation cycle is a timestep for the software to determine and update information used to keep the kinetic balance of the model through all calculation processes. It is different from the loading cycle and presents no physical significance.

Stage 3: Lower the sleeper 4 mm back to it's initial location. This process is used to calculate the force behaviour after settlement.

3.3.2. 2D model

It is challenging to use 3D FEM simulations to study long-term ballast settlement. Thus, as an alternative, a series of 2D DEM simulations were used. The 2D model contained particles simplified as ball shapes to maximise computational efficiency. 3D simulations were used to calibrate the 2D model and thus ensure accuracy. The 3D model is comprised the following key parts:

The ballast box is built using wall elements and had dimensions: 600*500 mm. The ballast layer was 450 mm in total, where 350 mm is under the bottom of the mono-block sleeper (or the bottom of the cubic part of the wedged sleeper), and 100 mm is filling in the crib.

The ballast particles are simulated using ball elements.

The wedged sleepers are built using wall elements, according to the cross-section of KLP sleeper type 202, which is a High-Density Poly-ethylene Polymer developed by Lankhorst and used as the prototype in the IN2ZONE project. The main part of wedged sleeper (also the mono-block sleeper) is 150 mm*250 mm. The only wedge considered was the 45 degrees case, which has a height of 125 mm.

The contact model is linear, capable of considering rolling resistance. The rolling resistance can simulate the interlock between particles, thus compensating for the loss of using ball particles.

The 2D model is shown in Fig. 9, and the contact parameters are shown in Table.2.

Due to the characteristics of the DEM wall elements, the sleepers could not obtain an acceleration for an unbalanced force [47]. Therefore a suitable loading method was important to simulate the long-term behaviour under repeated loading from the train and the positional restriction from the rail/fasteners. The loading approach was the displacement and force double-controlled method, which is described in the following 4 stages, and Fig. 10:

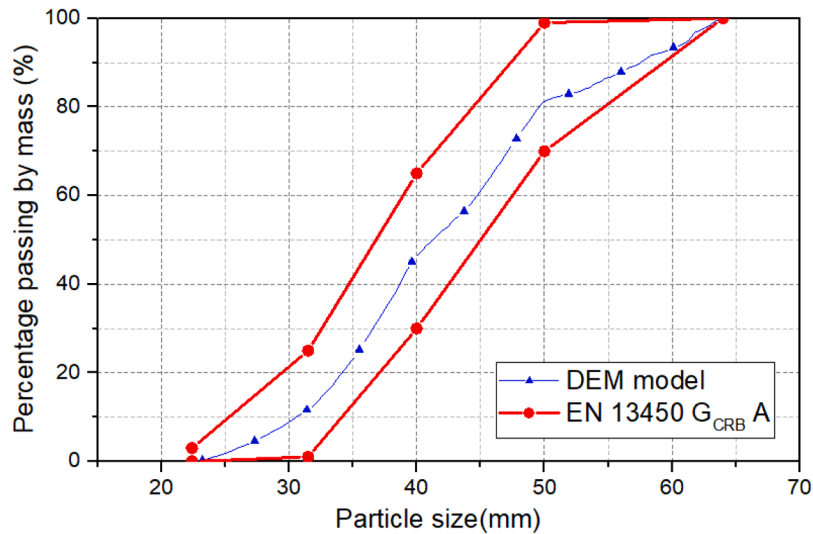**Step1**: Lift the sleeper 5 mm to produce an initial settlement.

Step2: Set a downward velocity (4 mm/s) on the sleeper. Stop the
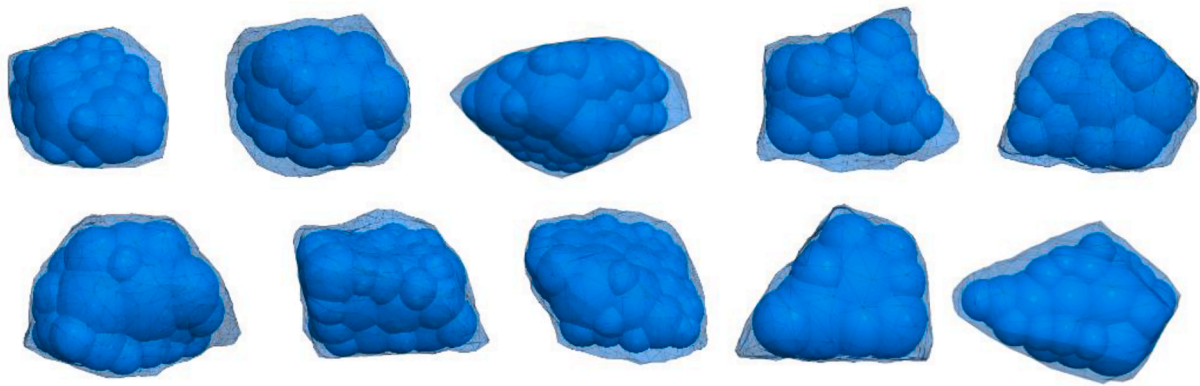
(a)

(b)

(c)

Fig. 6. DEM ballast particle size distribution, (a) Ballast particle Templates, (b) 3D scanning of ballast shape, (c) Particle size distribution.

sleeper when the ballast-sleeper contact force reaches 40kN (corresponding to the contact force in [6]). This step is force controlled, aiming to simulate the process when a wheel passes and produces loading on the sleeper.

Step 3: Reverse the velocity direction (so now upward 4 mm/s). Stop the sleeper when it reaches the location from step 1. In this step, the sleeper movement is displacement controlled, aiming to simulate the process when wheels have passed the sleeper. At the end of this step, the

velocity is reversed downwards, thus prepared for next loading.

Step 4: Repeat step 2 and step 3. Step 2 and step 3 combine together, making up the whole process of the train passage. After several cycles, the correction effect of the sleeper leads to a steady state. The total loading was around 500 cycles, and the calculation cycles were around 600 k.
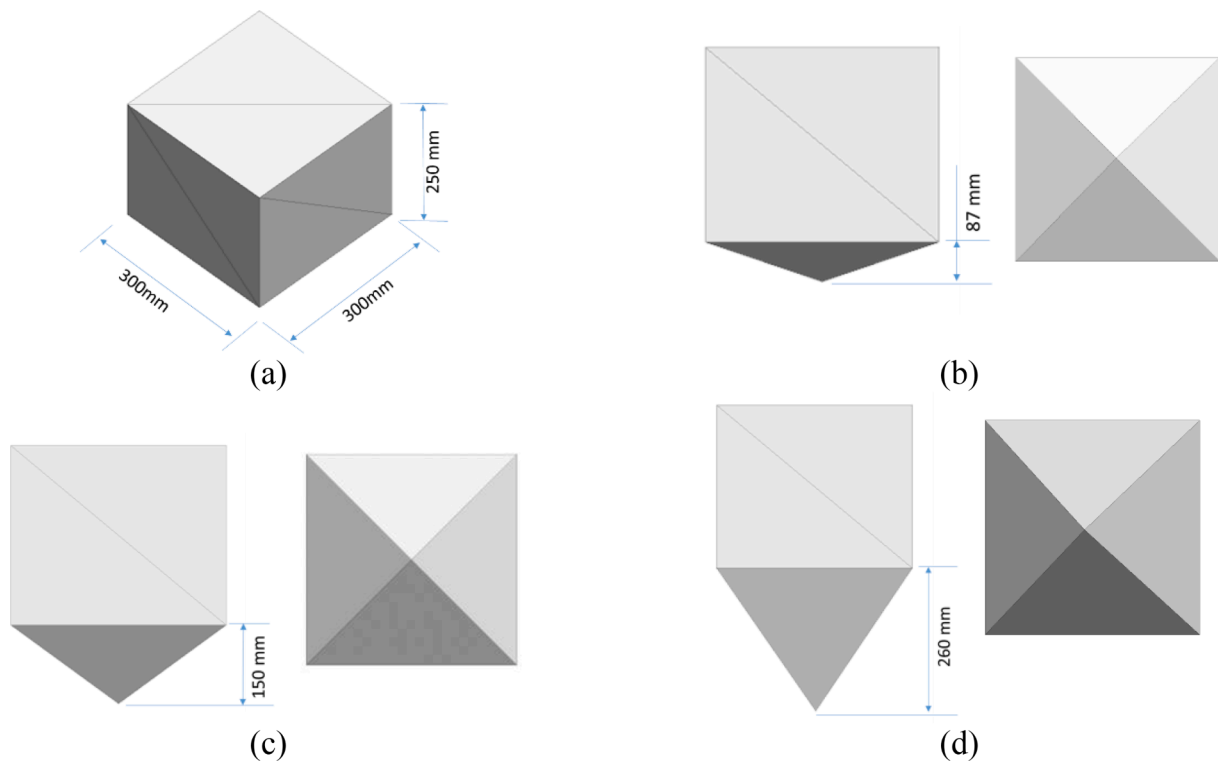
Fig. 7. Wedge sleepers designs used in the DEM model, (a) Mono-block sleeper, (b) 30-degree wedged sleeper, (c) 45-degree wedged sleeper, (d) 60-degree wedged sleeper.

Table 1
Linear contact model Parameters for ballast box model.

Parameters	Ballast (Clump)	Sleeper
Tangential stiffness(N/m)	$2e^8$	$5e^9$
Normal stiffness(N/m)	$2e^8$	$5e^9$
Friction coefficient	0.5	0.5
Mass density(kg/m^3)	2800	–
Damping coefficient	0.7	–

4. Analysis

4.1. Wedge sleeper type

The scaled laboratory tests were used to compare the different designs against the reference sleeper. The results of the final displacement of the sleepers are shown in Fig. 11. The sleeper displacement proves the function of the support correction. The smaller displacement of the wedged sleeper shows better correction under 10 mm initial settlement. Due to the tests lifting the bridge 10 mm as the initial settlement, and the ballast particle size is around 6 mm, the mono-sleeper also showed a 5.8 mm correction. In comparison, all the wedged sleepers showed a better correction effect than the mono-block sleeper. The correction of the 45-degree sleeper is approximately 7.4 mm, and the correction of 60-degree sleeper is approximately 8 mm.

The single-wedge showed no significant difference in displacement compared with the multi-wedge sleeper. After 16 runs, voids between the sleeper and ballast layer were observed between the wedges of the multi-wedged sleeper, as shown in Fig. 12. This phenomenon is mainly related to the complex contact surfaces of the multi-wedge sleeper. Only longitudinal ballast movement filled the void, but minimal lateral ballast movement (between the wedges, dark area in the red circle) contributed to the correction. Therefore the multi-wedged design was discarded and the remaining analyses focused on single-wedge solutions.

4.2. Wedge sleeper angle

To analyse the influence of wedge angle on the support correction effect, the contact behaviour between the sleeper and the ballast particles was obtained using 3D DEM simulations.

During the loading process, the displacement of the sleeper and the contact force between the sleeper and ballast were recorded. Fig. 13 shows the results corresponding to the 45-degree sleeper. Two points (Point a and Point b) and 1 range (Range c) were used to analyse the force performance of the wedge sleeper.

Point a: When the sleeper lifting process is finished and stops at the position represented for settlement. The biggest frictional force (z-direction) can be seen near this point. It presents the frictional interaction between the hanging sleeper and ballast.

Point b: The point where the contact force between the sleeper and particles begins to increase rapidly. Thus the displacement at this point can be regarded as ballast beginning to provide effective support. The global displacement at this point is an indicator. A higher value presents a better support correction.

Range c: The increase in contact force during the last 1 mm displacement in Stage 3. A higher value indicates a better support correction.

The contact forces of 30 and 60 degree wedge sleepers are shown in Fig. 14, and detailed results are concluded in Table 3, which reflects the support correction effect due to the different angles. When the wedge angle increased from 30 degrees to 45 degrees, the sleeper displacement at point b increased from 0.86 mm to 1.51 mm. When the wedge angle was 60 degrees, the sleeper displacement was 2.36 mm. These results demonstrate that a bigger wedge angle led to a better settlement correction.

The correction is related to the angle of repose for ballast, which is normally observed to range from 30 to 45 degrees [40,48,49]. When the slope of the ballast-sleeper interface is higher than that range, ballast particles have the freedom to migrate into the ballast-sleeper void. This statement also explains why an increased correction effect occurred with
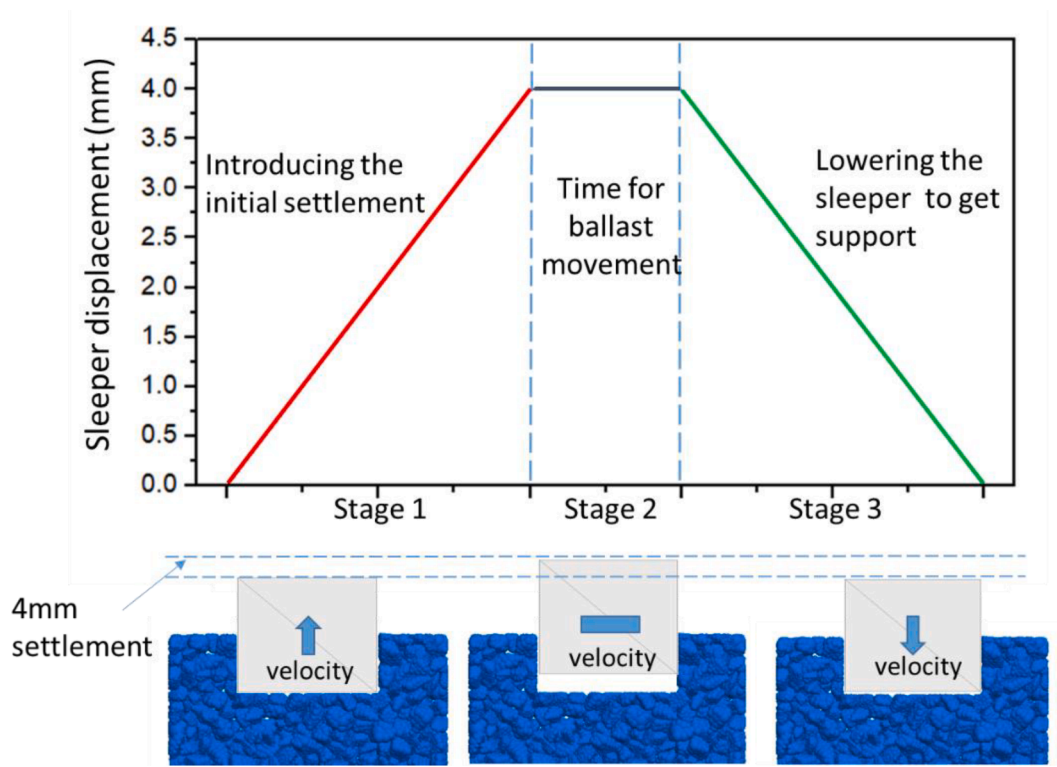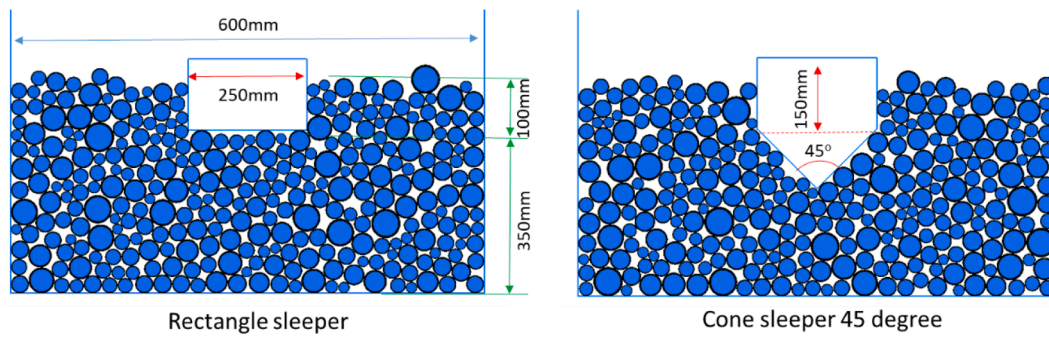
Fig. 8. Loading process in 3D DEM simulations.

Fig. 9. 2D ballast box model.

Table 2
Contact parameters for 2D model.

Parameters	Ballast (Ball)	Sleeper
Tangential stiffness(N/m)	5e^8	1e^9
Normal stiffness(N/m)	2e^8	1e^9
Friction coefficient	0.5	0.5
Rolling resistance coefficient	0.3	–
Mass density(kg/m^3)	2800	–
Damping coefficient	0.7	–

the angle increase. The correction increase from 30 to 45 degrees, or from 45 to 60 degrees, is much higher than that from 0 to 30 degrees. In addition, because the sleeper is displacement controlled, the peak contact force, maximum force and the force increase in the last 1 mm are all increased along with the angle increase. This behaviour shows that a higher angle can lead to better support.

Note that the settlement came from the upward sleeper lifting in the simulations. In contrast direction, the settlement comes from the ballast deformation in reality. So, the higher peak contact forces on the wedge
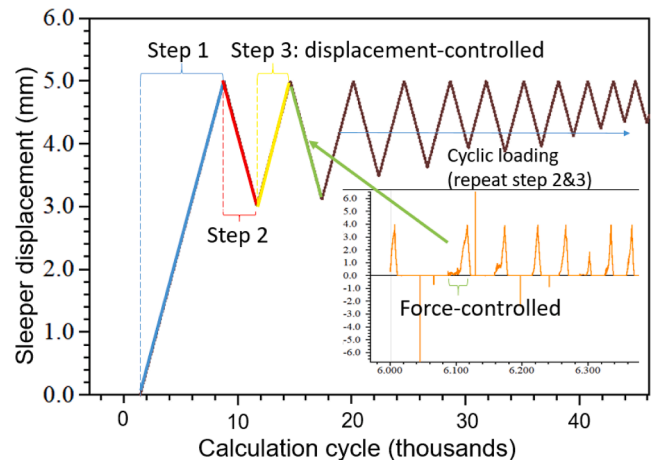

Fig. 10. Loading process of the 2D model.

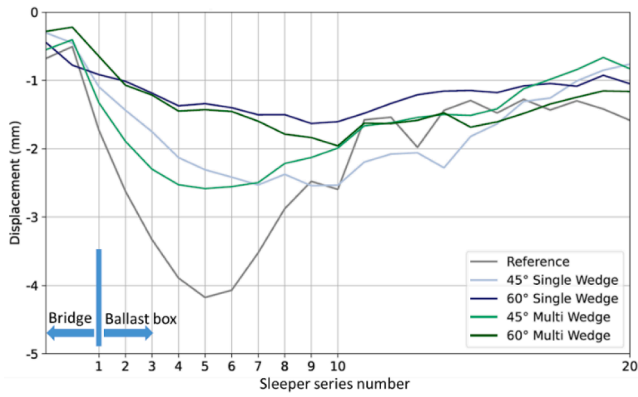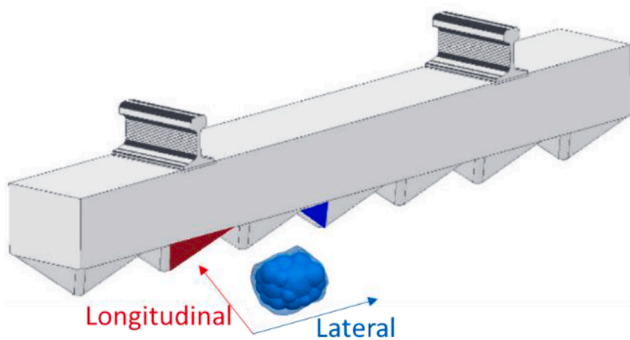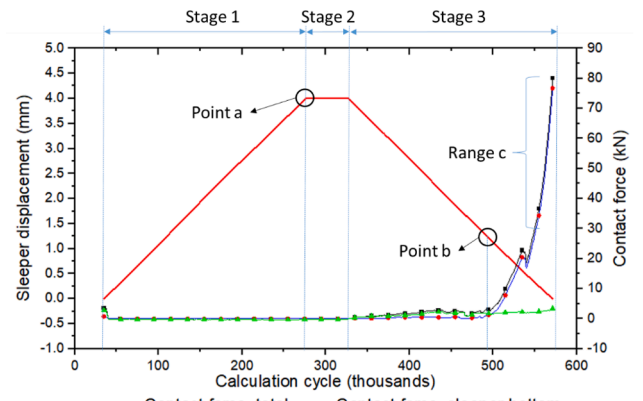Fig. 11. Final sleeper displacement under 10 mm initial settlement.
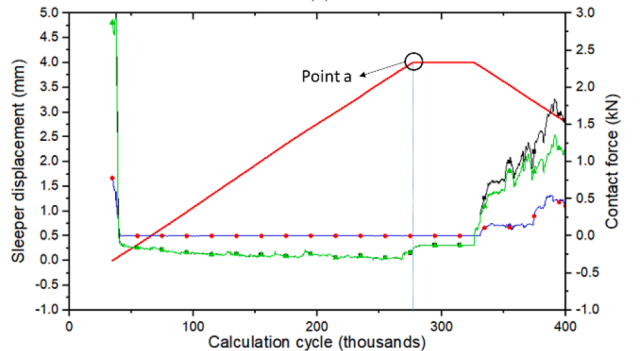

(a)

(b)

Fig. 12. Voiding under multi-wedged sleeper after 16 runs, (a) Laboratory tests, (b) Schematic diagram.

(a)

(b)

(c)

Fig. 13. Sleeper displacement and contact force for the 45-degree wedged sleeper, (a) Sleeper displacement and contact force, (b) Stages 1 & 2 (zoomed), (c) Stage 3 (zoomed).

sleeper are caused by the higher compaction when compelling the sleepers back to a designed position. The extra high contact forces will not appear because the real settlement pattern will not produce extra compaction between sleeper and ballast.
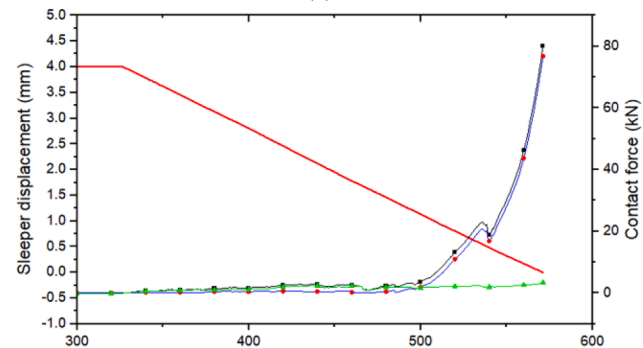
However, the mono-block sleeper also can be regarded as a 90 degree wedge, which may produce the steepest slope for ballast particles to slide into the void. The results do not prove the hypothesis because under the same settlement, the mono-block sleeper provides a smaller void and the possible restriction on ballast, compared with wedged sleeper. The void under the sleeper is related to both settlement and the

wedge angle, as shown in Fig. 15. In addition, the side of the mono-block restricts ballast rotation and displacement.

The maximum contact forces are shown in Fig. 16, which are 8.66 kN, 21.85 kN, and 48.20 kN, corresponding to 30, 45, and 60-degree wedged sleepers, and 3.92 kN of the mono-block sleeper, respectively. The increase of maximum contact force shows an increasing trend. It was in accordance with the increasing wedge angle and proved that a higher wedge angle leads to better support. As for the ballast-sleeper contact force distribution, the maximum contact forces (red dot in Fig. 16) are observed on the slope of the wedge. In contrast, the maximum contact forces of the mono-block sleeper are observed at the edge of the bottom.
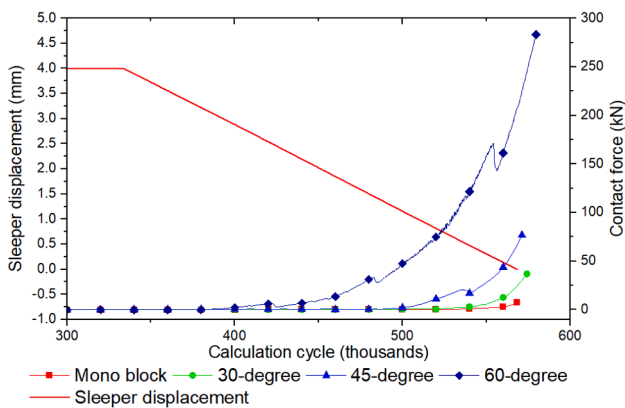
A higher angle leads to improved support correction behaviour, force
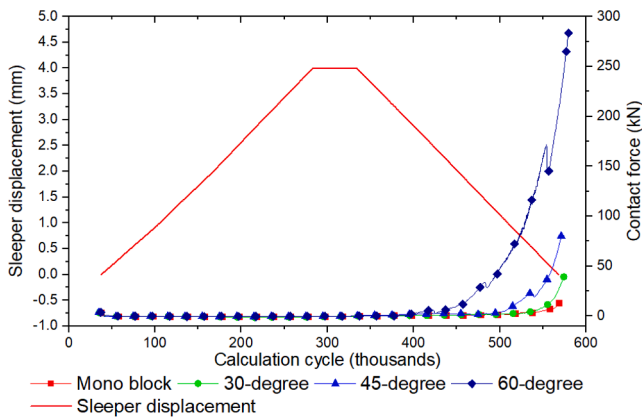
(a)
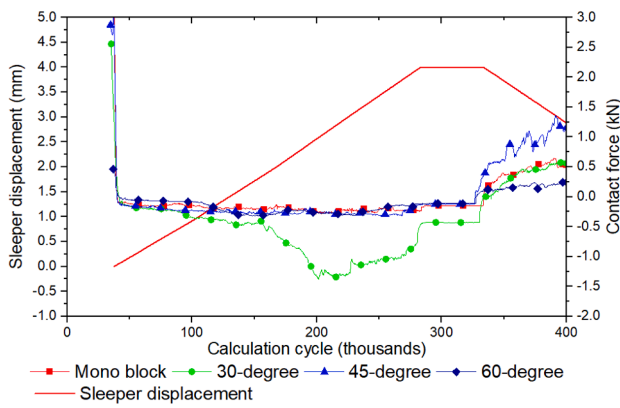
(b)

(c)

Fig. 14. Sleeper displacement and contact force on different sleepers, (a) Total process, (b) Stages 1 & 2 (zoomed), (c) Stage 3 (zoomed).

Table 3
Key results of wedged sleeper.

Wedge angle (degree)	Biggest frictional force (Z-direction) (N)	Displacement when sleeper begins to get support (mm)	Force increase in last 1 mm (kN)	Peak sleeper contact force (Z-direction) (kN)
30	−0.14	0.86	1.56	39.31
45	−0.32	1.51	74.95	80.12
60	−0.34	2.36	21.88	284.33
Mono-block sleeper	−0.29	0.98	11.71	13.49

(a)

(b)

Fig. 15. Ballast in the void after settlement, (a) wedged sleeper, (b) mono-block sleeper.

distribution, and maximum contact force. However, the effective ballast thickness for the 60-degree wedged sleeper is less than 100 mm, which is not enough to provide resilience [50]. Thus, 45 degrees was selected as the solution to take forward for the long-term settlement analysis.
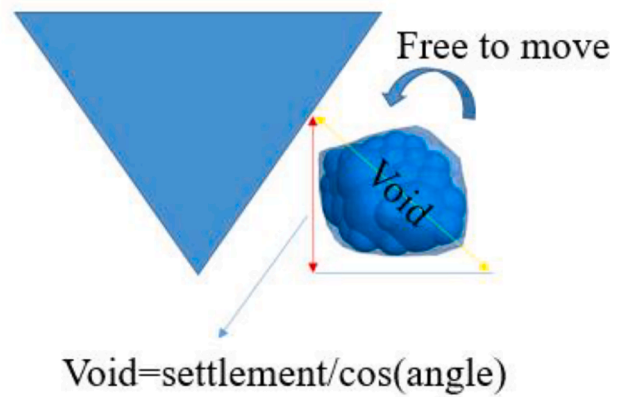
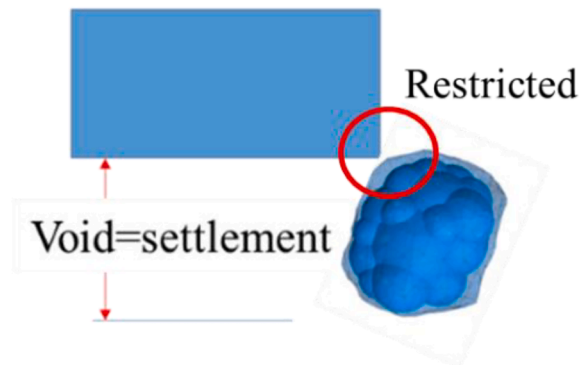### 4.3. Settlement behaviour

4.3.1. 2D model calibration

2D DEM simulations were used to study longer-term settlement behaviour instead of 3D simulations due to the efficiency problem. The 2D models are time-saving, making the long-term analysis to be possible, but accuracy is low. The calculation shows that even if the same parameters are used to build models, results still vary. Thus, each condition (different sleepers under different settlements) is calculated 20 times. Then the contact force results, especially the force distribution of the 3D model, are used to calibrate the 2D model.

The calibration is to distinguish and discard the failure model. For example, the contact force distribution and displacement results in Fig. 17 show a representative model of failure calculation. The force and compaction status of ballast are against the results of 3D simulations.

Note that the curve shape in Fig. 17b is similar to that shown in Fig. 10, but it contains around 500 loading cycles (8.2 million calculation cycles) in a limited axle length, thus leading to a dense and black layout. As an explanation, the curve contains 4 parts:
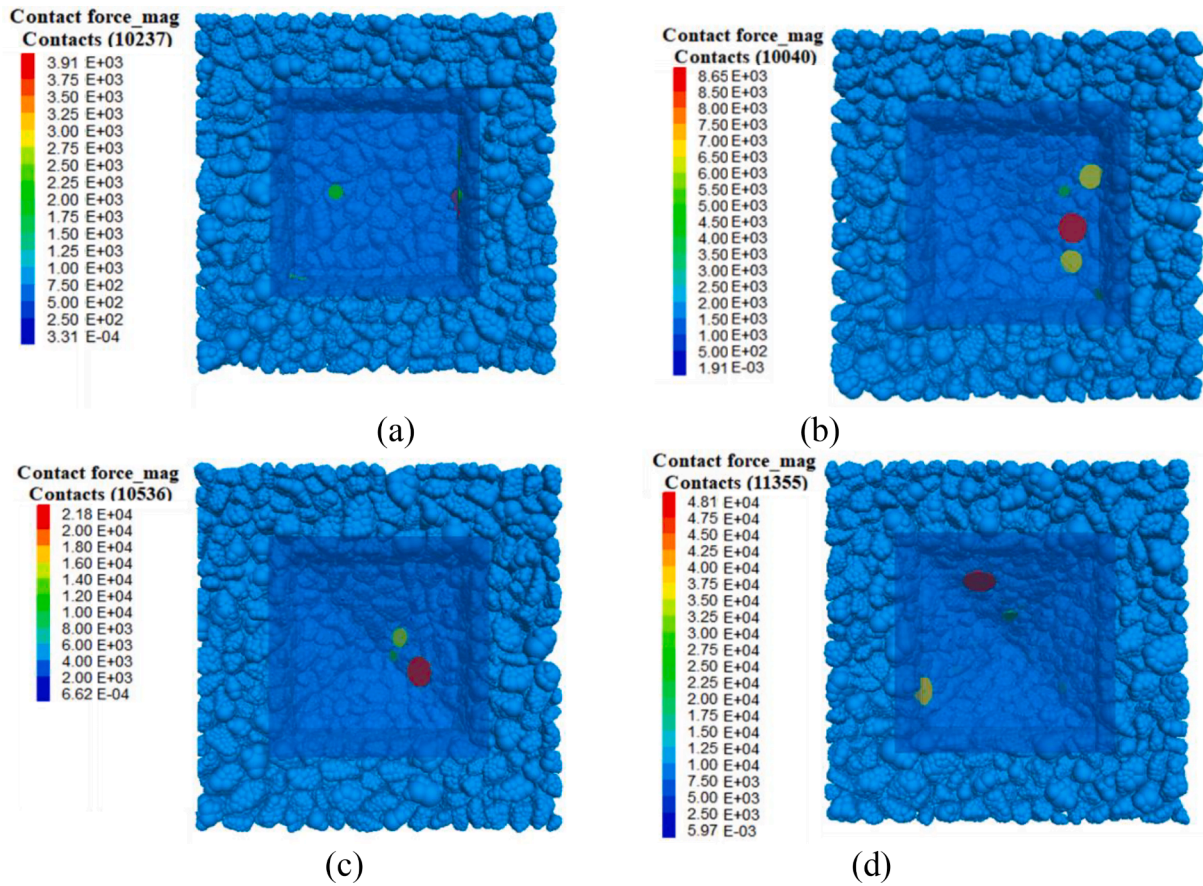
Fig. 16. Contact force on sleeper (unit: N). (a) Mono-block sleeper (b) 30-degree wedged sleeper, (c) 45-degree wedged sleeper, (d) 60-degree wedged sleeper.
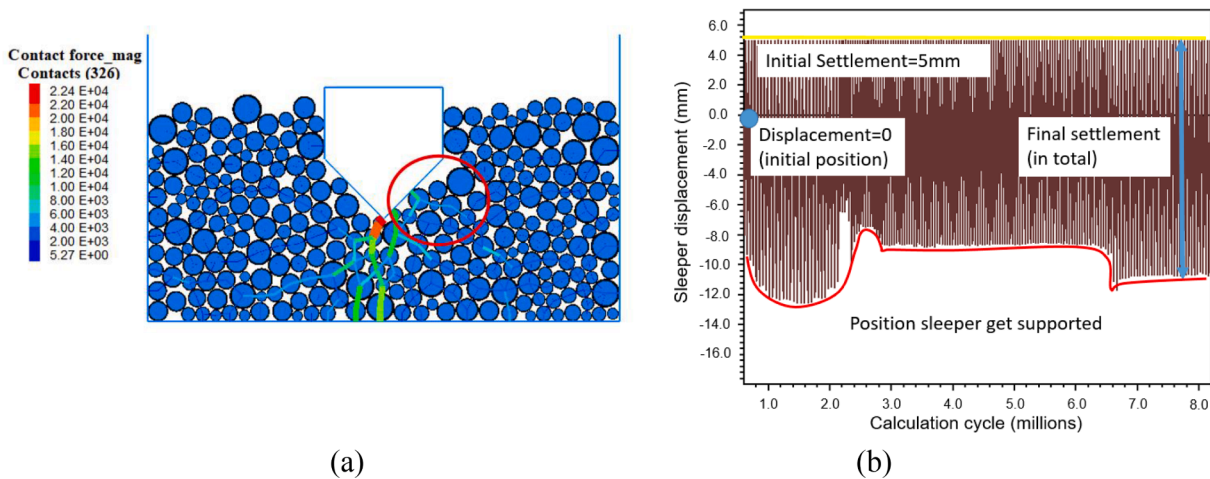

Fig. 17. A case of wedged sleeper with bad correction, (a) Contact force distribution (unit: N), (b) Sleeper displacement (unit: m).

1) The zero point is the sleeper location before settlement;
2) The top yellow line is the location of the sleeper after the initial settlement. The location is fixed because of the restriction of the fastening system and rail;
3) The red bottom line is the location of the sleeper when the loading (of the wheel) is fully applied on the sleeper;
4) The distance between the yellow line and the red line is the settlement under cyclic loading.

In detail, the settlement of the failure model is 16 mm in total, and no settlement correction through all the loading cycles. This behaviour is caused by the contact between the sleeper bottom and the ballast is uncompacted. In addition, the maximum contact force is 2.25kN, which is observed at the tip of wedged sleeper, but this peak force did not appear in the 3D model (Fig. 16). All of the force and compaction status of ballast are against the results of 3D simulations. For this reason, this simulation is considered to be an failure then discarded.

A representative 2D model, whose results are in accordance with 3D results, are shown in Fig. 18. In this case, the settlement correction happens at the very beginning of the cyclic loading, the final correction is more than 4 mm, and the sleeper is stable through the cyclic loading process. The maximum contact force is 13.9kN. The contact force
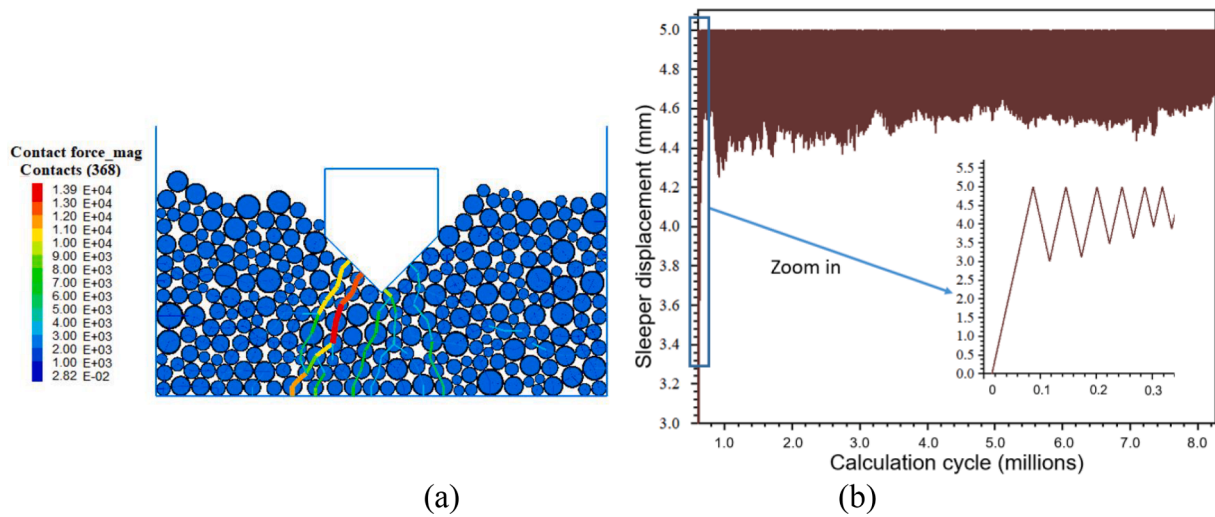
Fig. 18. A case of wedged sleeper with good correction, (a) Contact force distribution (unit: N), (b) Sleeper displacement (unit: m).
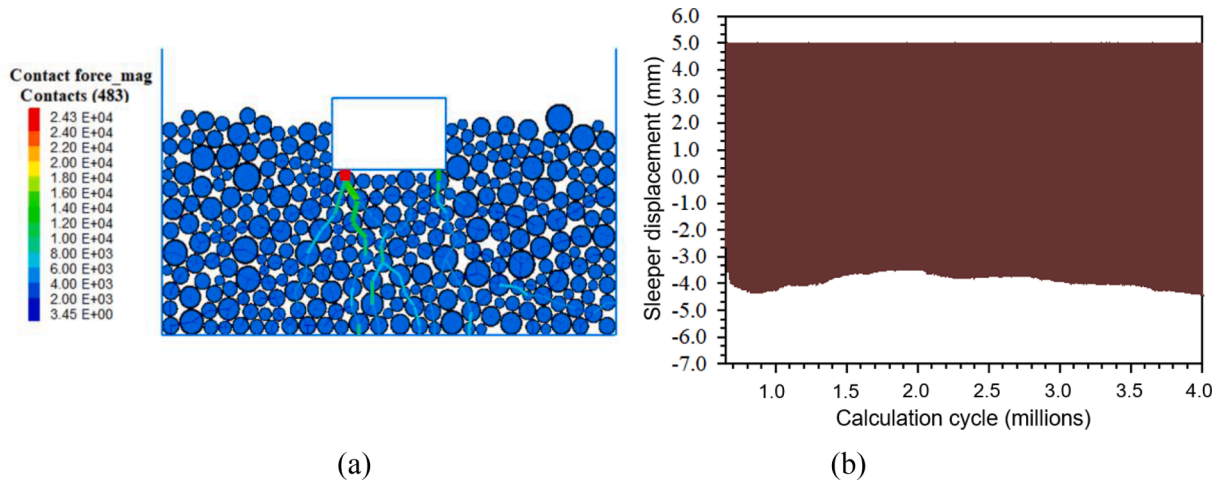

Fig. 19. A case of mono-block sleeper, (a) Contact force distribution (unit: N), (b) Sleeper displacement (unit: m).

Table.4
Results of the 2D model under 5 mm initial settlement.

Sleeper type	Correction (mm)	Final settlement (mm)	Maximum contact force (kN)
Mono-block sleeper	−4.3	9.3	24.31
	−3.8	8.8	37.96
	−4	8	17.57
Wedged sleeper	5	0	18.49
	4	1	23.40
	5	0	13.94

distribution is similar to that of the 3D ballast box model (Fig. 16). Both the force distribution and maximum contact force are in accordance with the 3D simulations. This model is accepted for further analysis.

For the mono-block sleeper, the model and results are also calibrated by the results of 3D models, although most of the 2D results are at a similar level. Among them, a representative result is shown in Fig. 19. The correction effect is not observed. The maximum force appears near the edge of the sleeper bottom. The force distribution and maximum contact force are in accordance with the 3D simulations.

The DEM simulations provide both mesoscopic results and macroscopic results. In the 3D models, the particle shape and contact behaviour were verified in the author's previous research. By the calibration,

the mesoscopic results of 2D models are qualified, then the failure model is discarded, and the left 2D models show similar results in mesoscopic. Because the macroscopic results are the external appearance of mesoscopic behaviour, those 2D models are also verified by the 2D/3D calibration.

4.3.2. Settlement behaviour

As mentioned above, the 2D models are calibrated according to the results of 3D models. The results of the accepted models are listed in Table 4. The 3 representative results are selected to show the deviation according to the force range. Those are the biggest value, the middle value, and the minimum value of the maximum contact force. Note that the negative value means no correction, but a further settlement beyond the initial setting is observed after the loading process.

The settlement of mono-block sleeper after cyclic loading is 8 mm to 9.3 mm, whereas the settlement of wedged sleeper is only 0 mm or 1 mm. The maximum contact force for the mono-block sleeper range from 17.57 kN to 37.96 kN, whereas the maximum contact force of wedged sleeper range from 13.94 kN to 23.40 kN, the decrease ratio is around 20% to 38%. In addition, the force distribution area of a mono-block sleeper is much smaller than the wedged sleeper (as shown in Fig. 18 and Fig. 19). That is to say, the wedged sleeper not only provides a support correction effect but also decreases the maximum force.

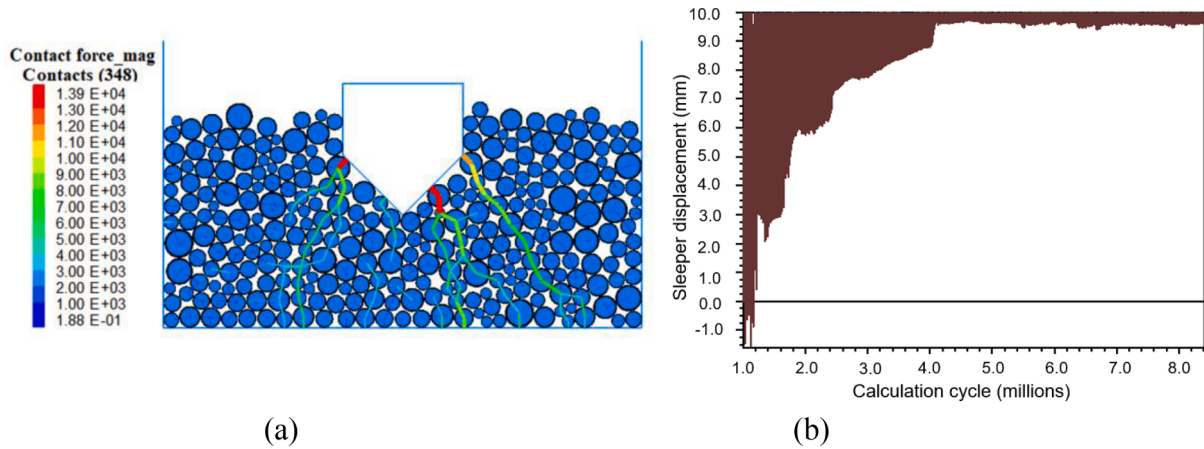Further, a calibrated 2D model is employed to analyse the correction

Fig. 20. A case of wedged sleeper with good correction under 10 mm settlement. (a) Contact force distribution (unit: N), (b) Sleeper displacement (unit: m).

Fig. 21. A case of wedged sleeper with good correction under 15 mm settlement. (a) Contact force distribution (unit: N), (b) Sleeper displacement (unit: m).

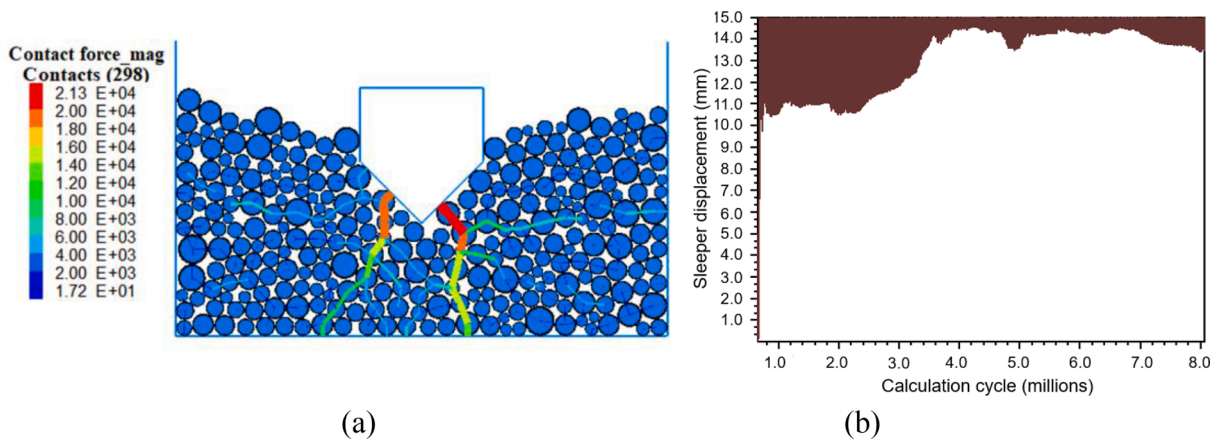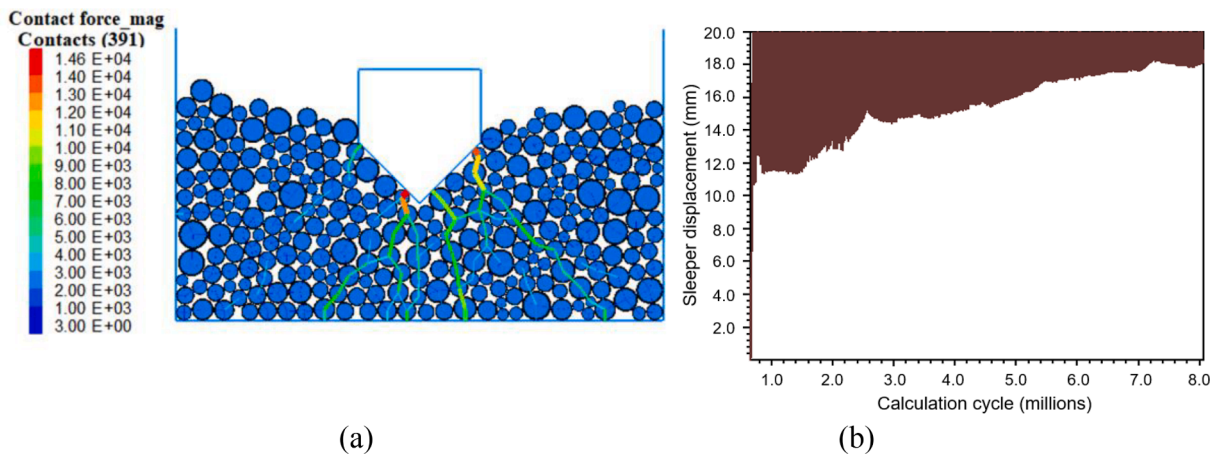

Fig. 22. A case for wedged sleeper with good correction under 20 mm settlement. (a) Contact force distribution (unit: N), (b) Sleeper displacement (unit: m).

Table 5
Correction for higher settlement.

Settlement (mm)	Correction (mm)	Maximum contact force (kN)
10	10	14.0
15	14	21.31
20	18	14.60

effect under a higher settlement. The initial settlement is enlarged to 10 mm, 15 mm and 20 mm, and the results are listed in Figs. 20 to 22 and Table 5. Results show that the wedged sleeper can correct all the settlements under 5 mm and 10 mm conditions. When the settlement increases to 15 mm and 20 mm, the correction is still effective, and the force behaviour is similar to that of cases under 5 mm settlements.

5. Conclusions

Railway track transition zones are areas with rapidly changing track stiffness. It is common for hanging sleepers to develop on the softer side due to differential settlement. To address this problem, this paper proposed and investigated a new concept sleeper with a wedge-shaped geometry. First, scaled laboratory tests are used to study the performance of difference wedge geometries, and it is found that a single long wedge is preferable compared to multiple smaller wedges. Next, 3D DEM simulations are performed to analyse the contact forces in the ballast due to different single wedge designs. Finally, 2D DEM simulations are performed to study the long-term settlement behaviour. The main conclusion were:

1. When the bottom angle of wedged sleeper is larger than the repose angle of ballast material, particles have the freedom to migrate into the settlement induced voids
2. An increased wedge sleeper angle stimulates greater particle migration and thus improved, the support correction. However the longer wedge also leads to a decrease in effective ballast height under sleeper.
3. The ability of wedge-shaped sleepers to reduce the presence of sleeper voids is promising, however further study is needed.
4. Compared with the mono-block sleeper, the wedged sleeper reduces the contact force between the sleeper and the ballast due to a wider contact area.

Following with the paper finished, the full-scale (45-degree) wedge sleeper was produced. The long-term behaviour was analysed based on a series of large-scale laboratory tests. Primary results were obtain, which are in accordance with the results of numerical simulations. Further works and optimisation of the sleeper is ongoing.

CRediT authorship contribution statement

Wenli Jia: Simulation, Analysis, Writing, Editing. **Valeri Markine:** Supervision, Methodology, Reviewing. **Mario Carvalho:** Laboratory tests. **David P. Connolly:** Supervision, Reviewing. **Yunlong Guo:** Supervision.

Declaration of Competing Interest

The authors declare the following financial interests/personal relationships which may be considered as potential competing interests:

Wenli Jia, Valeri Markine, Mario Carvalho, David P. Connolly, Yunlong Guo reports financial support was provided by European Commission.

Data availability

Data will be made available on request.

Acknowledgments

References

[1] R. Sañudo, L. dell'Olio, J.A. Casado, I.A. Carrascal, S. Diego, Track transitions in railways: a review, Constr. Build. Mater. 112 (2016) 140–157.
[2] J.-A. Zakeri, V. Ghorbani, Investigation on dynamic behavior of railway track in transition zone, J. Mech. Sci. Technol. 25 (2) (2011) 287–292.
[3] A. Paixão, E. Fortunato, R. Calçada, Design and construction of backfills for railway track transition zones, Proc. Inst. Mech. Eng., Part F: J. Rail Rapid Transit 229 (1) (2013) 58–70.
[4] H. Wang, V. Markine, Modelling of the long-term behaviour of transition zones: prediction of track settlement, Eng. Struct. 156 (2018) 294–304.
[5] H. Huang, B. Brennecke, Track stiffness transition zone studied with three-dimensional sandwich track model, Transp. Res. Rec.: J. Transp. Res. Board 2374 (1) (2013) 136–142.
[6] H. Wang, V. Markine, Dynamic behaviour of the track in transitions zones considering the differential settlement, J. Sound Vib. 459 (2019), 114863.
[7] C. Charoenwong, D.P. Connolly, P.K. Woodward, P. Galvín, P. Alves Costa, Analytical forecasting of long-term railway track settlement, Comput. Geotech. 143 (2022), 104601.
[8] C. Charoenwong, D.P. Connolly, K. Odolinski, P. Alves Costa, P. Galvín, A. Smith, The effect of rolling stock characteristics on differential railway track settlement: an engineering-economic model, Transp. Geotech. 37 (2022) 100845.
[9] D. Li, D. Otter, G. Carr, Railway bridge approaches under heavy axle load traffic: problems, causes, and remedies, Proce. Inst. Mech. Eng., Part F: J. Rail Rapid Transit 224 (5) (2010) 383–390.
[10] M. Sol-Sánchez, F. Moreno-Navarro, M.C. Rubio-Gámez, Viability analysis of deconstructed tires as material for rail pads in high-speed railways, Mater. Des. 64 (2014) 407–414.
[11] T. Xin, Y. Ding, P. Wang, L. Gao, Application of rubber mats in transition zone between two different slab tracks in high-speed railway, Constr. Build. Mater. 243 (2020), 118219.
[12] Y. Çati, S. Gökçeli, Ö. Anil, C.S. Korkmaz, Experimental and numerical investigation of USP for optimization of transition zone of railway, Eng. Struct. 209 (2020), 109971.
[13] M. Esmaeili, M. Siahkouhi, Tire-derived aggregate layer performance in railway bridges as a novel impact absorber: numerical and field study, Struct. Control Health Monit. 26 (10) (2019) e2444.
[14] P. Chumyen, D.P. Connolly, P.K. Woodward, V. Markine, The effect of soil improvement and auxiliary rails at railway track transition zones, Soil Dyn. Earthq. Eng. 155 (2022), 107200.
[15] R. David, L. Dingqing, Design of Track Transitions, The National Academies Press, Washington, DC, 2006.
[16] A. Namura, T. Suzuki, Evaluatin of countermeasures against differential settlemenr at track transitions, Quart. Rep. RTRI 48 (3) (2007) 176–182.
[17] W. Li, X. Bian, Dynamic performance of pile-supported bridge-embankment transition zones under high-speed train moving loads, Procedia Eng. 143 (2016) 1059–1067.
[18] Y. Qian, E. Tutumluer, Y.M.A. Hashash, J. Ghaboussi, D.D. Davis, Ballast settlement ramp to mitigate differential settlement in a bridge transition zone, Transp. Res. Rec.: J. Transp. Res. Board 2476 (1) (2015) 45–52.
[19] B. Indraratna, M.A. Shahin, W. Salim, Use of geosynthetics for stabilizing recycled ballast in railway track substructures, Proceedings of NAGS2005/ GRI 19 Cooperative Conference (2015) 1-15.
[20] B. Indraratna, S. Nimbalkar, T. Neville, Performance assessment of reinforced ballasted rail track, Proceedings of the ICE: Ground Improvement 167(1) (2014) 24-34.
[21] B. Indraratna, M.M. Biabani, S. Nimbalkar, Behavior of geocell-reinforced subballast subjected to cyclic loading in plane-strain condition, J. Geotech. Geoenviron. Eng. 141 (1) (2015) 04014081.
[22] G. Jing, L. Qie, V. Markine, W. Jia, Polyurethane reinforced ballasted track: Review, innovation and challenge, Constr. Build. Mater. 208 (2019) 734–748.
[23] P. Schneider, R. Bolmsvik, J.C.O. Nielsen, In situ performance of a ballasted railway track with under sleeper pads, Proc. Inst. Mech. Eng., Part F: J. Rail Rapid Transit 225 (3) (2011) 299–309.
[24] S. Kaewunruen, A. Aikawa, A.M. Remennikov, Vibration attenuation at rail joints through under sleeper pads, Procedia Eng. 189 (2017) 193–198.
[25] M. Sol-Sánchez, F. Moreno-Navarro, M.C. Rubio-Gámez, Analysis of ballast tamping and stone-blowing processes on railway track behaviour: the influence of using USPs, Géotechnique 66 (6) (2016) 481–489.
[26] H. Wang, V. Markine, Corrective countermeasure for track transition zones in railways: adjustable fastener, Eng. Struct. 169 (2018) 1–14.
[27] K. Muramoto, T. Nakamura, T. Sakurai, A study of the effect of track irregularity prevention methods for the transition zone between different track structures, Quart. Rep. RTRI 53 (4) (2012) 211–215.
[28] K. Muramoto, T. Nakamura, T. Sakurai, A Hanging Sleepers Preventing Method using Automatic Irregularity-Correcting Short Sleeper, 11th World Congress on Railway Research, (2016).
[29] P. Insley, P. Sharpe, Self-compensating sleeper and method of maintaining a railroad track, 2020, Europe, Patent No. EP3608472A1.
[30] S.H. Lee, J.W. Lee, C.Y. Choi, H.J. Jang, Automatic subsidence correcting apparatus for loose sleeper between different track structures, and constructing method thereof. Korea, Patent No. KR101374526B1;KR20130137465A.
[31] S.H. Lee, J.W. Lee, Rail tie having embedded automatic differential settlement compensation apparatus using oil pressure for railroad tracks, 2014, Korea, Patent No. EP3112533A1;EP3112533A4;EP3112533B1;KR101625841B1; KR20150100338A;US10138604B2;US2017009405A1;WO2015129996A1.
[33] C. Calla, Two layered ballast system for improved performance of railway track, Coventry University, (2003).
[33] T. Abadi, L.L. Pen, A. Zervos, W. Powrie, Improving the performance of railway tracks through ballast interventions, Proc. Inst. Mech. Eng., Part F: J. Rail Rapid Transit 232 (2) (2016) 337–355.
[34] P. Claisse, M. Keedwell, C. Calla, Tests on a two-layered ballast system, Proc. Inst. Civ. Eng. – Transp. 156 (2) (2003) 93–101.
[35] H. Li, G. McDowell, Discrete element modelling of two-layered ballast in a box test, Granul. Matter 22 (4) (2020).

[36] G.Q. Jing, P. Aela, H. Fu, H. Yin, Numerical and experimental analysis of single tie push tests on different shapes of concrete sleepers in ballasted tracks, Proc. Inst. Mech. Eng., Part F: J. Rail Rapid Transit 233 (7) (2018) 666–677.

[37] Y. Guo, H. Fu, Y. Qian, V. Markine, G. Jing, Effect of sleeper bottom texture on lateral resistance with discrete element modelling, Constr. Build. Mater. 250 (2020) 118770.

[38] X. Zhang, C. Zhao, W. Zhai, DEM Analysis of Ballast Breakage Under Train Loads and Its Effect on Mechanical Behaviour of Railway Track, in: Proceedings of the 7th International Conference on Discrete Element Methods, 2017, pp. 1323–1333.

[39] C. Chen, B. Indraratna, G. McDowell, C. Rujikiatkamjorn, Discrete element modelling of lateral displacement of a granular assembly under cyclic loading, Comput. Geotech. 69 (2015) 474–484.

[40] P. Aela, L. Zong, M. Esmaeili, M. Siahkouhi, G. Jing, Angle of repose in the numerical modeling of ballast particles focusing on particle-dependent specifications: parametric study, Particuology 65 (2022) 39–50.

[41] N.T. Ngo, B. Indraratna, C. Rujikiatkamjorn, Simulation ballasted track behavior: numerical treatment and field application, Int. J. Geomech. 17 (6) (2017) 04016130.

[42] Y. Guo, C. Zhao, V. Markine, G. Jing, W. Zhai, Calibration for discrete element modelling of railway ballast: a review, Transp. Geotech. 23 (2020) 100341.

[43] G. Jing, W. Jia, X. Wang, V. Markine, R. Nålsund, Y. Guo, Experimental and numerical study on lateral resistance of frictional sleeper with arrowhead groove, Transp. Geotech. 30 (2021), 100638.

[44] W. Jia, V. Markine, Y. Guo, G. Jing, Experimental and numerical investigations on the shear behaviour of recycled railway ballast, Constr. Build. Mater. 217 (2019) 310–320.

[45] G. Jing, X. Zhang, W. Jia, Lateral resistance of polyurethane-reinforced ballast with the application of new bonding schemes: laboratory tests and discrete element simulations, Constr. Build. Mater. 221 (2019) 627–636.

[46] Y. Guo, W. Jia, V. Markine, G. Jing, Rheology study of ballast-sleeper interaction with particle image Velocimetry (PIV) and discrete element modelling (DEM), Constr. Build. Mater. 282 (2021), 122710.

[47] I.C.G. Inc., PFC 5.0 document, (2018).

[48] J. Chen, R. Gao, Y. Liu, Numerical study of particle morphology effect on the angle of repose for coarse assemblies using DEM, Adv. Mater. Sci. Eng. 2019 (2019) 1–15.

[49] M.A. Wnek, E. Tutumluer, M. Moaveni, E. Gehringer, Investigation of aggregate properties influencing railroad ballast performance, Transp. Res. Rec.: J. Transp. Res. Board 2374 (1) (2013) 180–189.

[50] B. Indraratna, T. Ngo, Ballast Railroad Design: Smart-uow Approach, CRC Press, 2018.